ISSN 1674-1056
http://cpb.iphy.ac.cn
http://iopscience.iop.org/cpb
中国物理 B
Chinese Physics
中国物理 Chinese Physics B

Ultra-wideband low radar cross-section metasurface and its application on waveguide slot antenna array

Li-Li Cong(丛丽丽), Xiang-Yu Cao(曹祥玉), Tao Song(宋涛), Jun Gao(高军)

Citation: Chin. Phys. B . 2018, 27(11): 114101. **doi:** 10.1088/1674-1056/27/11/114101

Journal homepage: http://cpb.iphy.ac.cn; http://iopscience.iop.org/cpb

What follows is a list of articles you may be interested in

Ultra-thin circularly polarized lens antenna based on single-layered transparent metasurface

Kaiyue Liu(刘凯越), Guangming Wang(王光明), Tong Cai(蔡通), Wenlong Guo(郭文龙), Yaqiang Zhuang(庄亚强), Gang Liu(刘刚)

Chin. Phys. B . 2018, 27(8): 084101. **doi:** 10.1088/1674-1056/27/8/084101

A broadband cross-polarization conversion anisotropic metasurface based on multiple plasmon resonances

M Ismail Khan, Farooq A Tahir

Chin. Phys. B . 2018, 27(1): 014101. **doi:** 10.1088/1674-1056/27/1/014101

An electrically tunable metasurface integrated with graphene for mid-infrared light modulation

Zongpeng Wang(王宗鹏), Ya Deng(邓娅), LianFeng Sun(孙连峰)

Chin. Phys. B . 2017, 26(11): 114101. **doi:** 10.1088/1674-1056/26/11/114101

Ultra-wideband RCS reduction using novel configured chessboard metasurface

Ya-Qiang Zhuang(庄亚强), Guang-Ming Wang(王光明), He-Xiu Xu(许河秀)

Chin. Phys. B . 2017, 26(5): 054101. **doi:** 10.1088/1674-1056/26/5/054101

Ultra-thin two-dimensional transmissive anisotropic metasurfaces for polarization filter and beam steering application

Wen-Long Guo(郭文龙), Guang-Ming Wang(王光明), Hai-Peng Li(李海鹏), Kun Zhang(张昆), Tong Cai(蔡通)

Chin. Phys. B . 2016, 25(10): 104101. **doi:** 10.1088/1674-1056/25/10/104101

Ultra-wideband low radar cross-section metasurface and its application on waveguide slot antenna array*

Li-Li Cong(丛丽丽), Xiang-Yu Cao(曹祥玉)†, Tao Song(宋涛), and Jun Gao(高军)

Air Force Engineering University, Xi'an 710077, China

(Received 26 June 2018; revised manuscript received 27 July 2018; published online 25 October 2018)

A novel approach devoted to achieving ultra-wideband radar cross section reduction (RCSR) of a waveguide slot antenna array (WGSAA) while maintaining its radiation performance is proposed. Three kinds of artificial magnetic conductors (AMCs) tiles consisting of three types of basic units resonant at different frequencies are designed and arranged in a novel quadruple-triangle-type configuration to create a composite planar metasurface. The proposed metasurface is characterized by low radar feature over an ultra-wideband based on the principle of phase cancellation. Both simulated and measured results demonstrate that after the composite metasurface is used to cover part of the antenna array, an ultra-wideband RCSR involving in-band and out-of-band is achieved for co- and cross-polarized incident waves based on energy cancellation, while the radiation performance is well retained. The proposed method is simple, low-cost, and easy-to-fabricate, providing a new method for ultra-wideband RCSR of an antenna array. Moreover, the method proposed in this paper can easily be applied to other antenna architectures.

Keywords: metasurface, polarization-independent artificial magnetic conductor (PIDAMC), waveguide slot antenna array (WGSAA), radar cross section reduction

PACS: 41.20.Jb, 73.20.Mf **DOI:** 10.1088/1674-1056/27/11/114101

1. Introduction

With the rapid development of stealth and detection technology, radar cross section reduction (RCSR), which is regarded as a quantitative determination of target stealth capability, has received increasing attention.[1–3] As indispensable devices targeting detection and communication, antennas must assure effective radiation of electromagnetic (EM) waves primarily, which is the major difference from common objects in terms of RCSR.

Low-loss metasurfaces (MSs) have been extensively studied due to their unique EM properties, which are not found in natural materials and which provide a promising approach to antenna RCSR without degrading their radiation performance.[3–20] Artificial magnetic conductors (AMCs),[4] holographic MSs,[5] and polarization converter[6] have been successfully applied to single antennas or antenna arrays. In particular, the AMC has been extensively investigated[7–11] due to its low profile, easy processing, and good conformal shape. By combing AMC and perfect electric conductor (PEC) in a chessboard configuration, a 180° phase difference between reflected waves from these two different tiles can be created.[3,12] Consequently, the destructive interference between reflected waves results in RCSR in a specular direction. However, the narrow in-band behavior of AMC structure resulting from its inherent resonant characteristic limits its wide application. Generally, there are two main methods proposed in previous researches to achieve broadband RCSR. One is to design broadband AMC structures by multilayers,[13] low relative permittivity and thick substrate,[14,15] and integration with active elements.[16] The other is to replace the conventional PEC tiles with another different AMC tiles to broaden the effective 180° phase differential bandwidth.[17–20] Nonetheless, the RCSR bandwidth is still limited and the aforementioned structures cannot work well at relatively low frequencies. Moreover, there are many other restrictions when it comes to antenna arrays, especially the restricted loading space between antenna elements and the limited RCSR bandwidth.

In this work, we focus on the ultra-wideband RCSR of waveguide slot antenna array (WGSAA) involving in-band and out-of-band simultaneously based on a novel composite MS. Three different AMC tiles resonant at different frequencies are arranged in a quadruple-triangle-type chessboard configuration to perform the ultra-wideband low-radar-cross-section (RCS) MS on the basis of destructive phase difference. Simulation and experimental results demonstrate that combined with the structure of the WGSAA itself, an ultra-wideband RCS involving in-band and out-of-band is reduced considerably for both co- and cross-polarized incident waves. The in-band RCSR for co-polarized incidence can reach up to over −5 dB. Meanwhile, the radiation performance is well maintained, proving the feasibility and capability of our design method.

*Project supported by the National Natural Science Foundation of China (Grant Nos. 61671464, 61701523, and 61471389).

†Corresponding author. E-mail: 1183068955@qq.com

© 2018 Chinese Physical Society and IOP Publishing Ltd

2. Design of proposed slot antenna array

2.1. Design principle of ultra-wideband MS

As shown in Fig. 1, the reference antenna is an 8×10 asymmetrical ridged waveguide slot antenna array (WGSAA), which is widely used in radar and communication systems due to its simple structure, good mechanical strength, high power capacity, and low side-lobe.[21] The reference antenna operates at 3.20 GHz with a distance between adjacent slots along the x-axis of $0.494\lambda_{3.2\text{GHz}}$. Apparently, the WGSAA is subjected to strong structural scattering due to its large planar metallic ground.

The working principle of ultra-wideband RCSR that is proposed in this paper is the backscattering cancellation, which further depends on the phase difference among different AMC tiles. Unlike the implementation in traditional chessboard configuration, the phase differences in this paper are created by three different AMC tiles resonant at different frequencies. Since the phase difference no longer relies on resonance, effective energy cancellation can be obtained over an ultra-wideband. To gain an insight into the RCSR mechanism, we choose a general MS array consisting of $M \times N$ elements as depicted in Fig. 2. When a plane wave normally impinges on such an array, the total scattering field is the superposition of the reflected energy from all $M \times N$ elements. Assuming that each of all elements presents an equal reflection pattern, on the basis of standard array theory,[4] then the total reflection can be determined by

$$\begin{aligned} &\boldsymbol{E}_{\text{rtotal}} \\ &= \boldsymbol{P} \cdot F_{\text{A}} \\ &= \boldsymbol{P} \cdot \sum_{m=0}^{M-1} \sum_{n=0}^{N-1} \mathrm{e}^{\mathrm{j}[km\Delta x \sin\theta\cos\varphi + kn\Delta y \sin\theta\sin\varphi + \phi(m,n)]}, \end{aligned} \tag{1}$$

where $\boldsymbol{P}$ is the element pattern, approximate to $\cos\theta$, F_{A} is the array factor, k is the wavenumber, Δx and Δy are the distances between adjacent elements along x- and y-directions, respectively, $\phi(m,n)$ is the phase of (m,n) element, and θ, φ are the elevation and azimuth angles of an incidence.

For normal incidence with (θ, φ) = (0, 0), once the reflection phase difference between adjacent elements is $\pm 180°$, the reflection can be totally canceled out. However, since the reflection phase varies with frequency, the 180° phase difference cannot be maintained over an ultra-wideband. Usually, a 10-dB RCSR is set to be a criterion to compare with the same-sized PEC surface, that is,

$$10\log(|\boldsymbol{E}_{\text{rtotal}}|^2/|\boldsymbol{E}_{\text{pec}}|^2) \leq -10 \text{ dB}. \tag{2}$$

Hence, the effective reflection phase difference is deduced to be

$$143° \leq |\Delta\phi| \leq 217°. \tag{3}$$

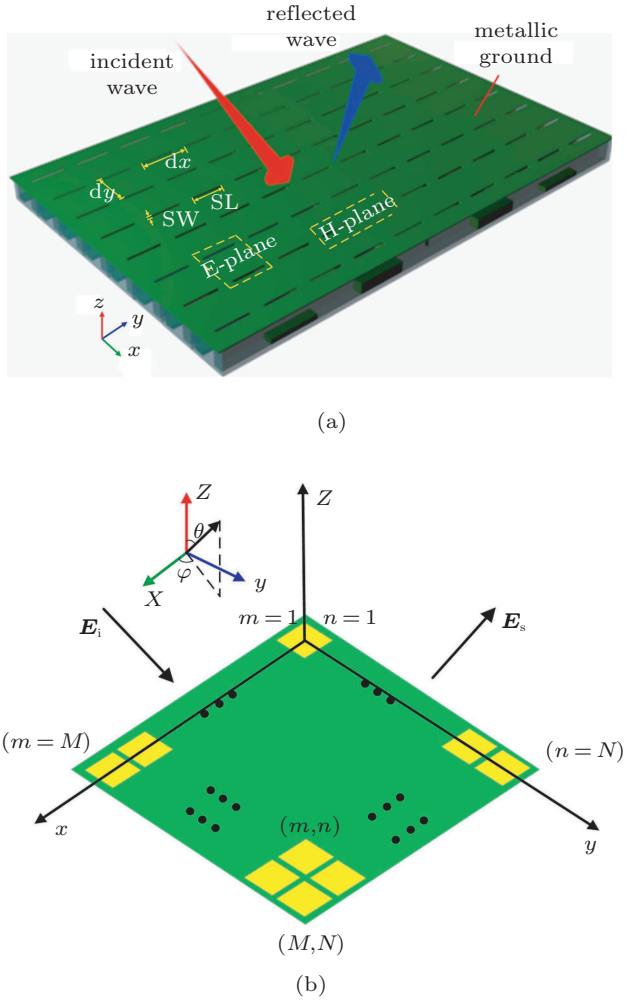


Fig. 1. (color online) Schematic diagram of (a) bare WGSAA and (b) $M \times N$ MS array.

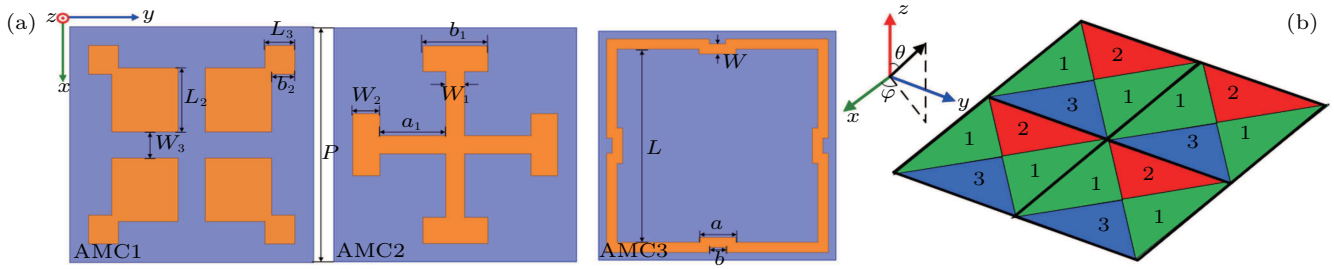


Fig. 2. (color online) (a) Geometry and dimensions of AMC1, AMC2, and AMC3. (b) Schematic view of quadruple-triangle arrangement. $P = 9$ mm, $a = 1.4$ mm, $a_1 = 2.45$ mm, $b = 0.6$ mm, $b_1 = 2.4$ mm, $b_2 = 0.86$ mm, $W = 0.4$ mm, $W_1 = 0.7$ mm, $W_2 = 1$ mm, $W_3 = 1$ mm, $L_1 = 7.6$ mm, $L_2 = 2.44$ mm, and $L_3 = 1.1$ mm.

Likewise, we set $180° \pm 30°$ as a criterion for the following analysis. Note that the backscattering cancellation is dependent on a dynamic variation of phase difference instead of a fixed value, and the RCSR bandwidth is consequently expected to expand to a large margin.

2.2. Design and analysis of PIDAMC

In 2007, Paguay *et al.*[3] first combined PEC and AMC in a chessboard arrangement to redistribute the reflected energy into four diagonal directions based on scattering cancellation. To broaden the RCSR bandwidth, two different AMC units were utilized in a chessboard configuration by Zhao *et al.*[8] However, the RCSR bandwidth was still limited. In 2014, Cui *et al.* proposed the concept "coding metamaterials".[22] When combined with antenna array, the restricted space between array elements cannot accommodate so many kinds of basic units. Consequently, the closely-spaced WGSAA resorts to an alternative method to address the problem of ultra-wideband RCSR.

Here, we choose three different AMC tiles resonate at different frequencies to achieve ultra-wideband RCSR. Each single sub-unit of the three different AMC tiles with detailed dimensions is depicted in Fig. 2(a), denoted as AMC1, AMC2, and AMC3, respectively. Each of the three sub-units is composed of two metallic layers separated by an exactly same-sized substrate with a dielectric constant of 2.65 and a loss tangent of 0.002. Moreover, despite of the top metallic layers with different shapes, all of the three sub-units are each backed by a full metallic ground to ensure no plane wave penetration. To create destructive interference in the largest bandwidth, full-wave numerical simulations have been carried out to optimize the parameters by using commercial simulation software Ansys HFSS. Floquet port excitations and master/slave boundaries are performed on each single sub-unit to simulate the infinite two-dimensional periodic boundary condition.

Figure 3 shows the reflection magnitudes and phases under the *x*- and *y*-polarized incidence for each sub-unit. As can clearly be observed, the magnitudes maintain 0.98 from 2 GHz to 21.5 GHz for both polarizations, indicating that the energy is almost reflected without absorption. The simulated results meet the requirement for phase cancellation principle. One can observe that AMC1 exhibits only one 0° reflection phase point at 10.9 GHz, while AMC2 and AMC3 demonstrate dual 0° reflection phase points at 7.15 GHz, 18 GHz and 3.98 GHz, 19.18 GHz, respectively. The different resonant statuses yield the destructive phase difference ranging over an ultra-wide band as depicted in Fig. 4. For normal incidence, the phase difference covering a range of $180° \pm 30°$ between every two of the three sub-units nearly ranges from 3.98 GHz to 18.84 GHz except from 4.2 GHz to 6.9 GHz.

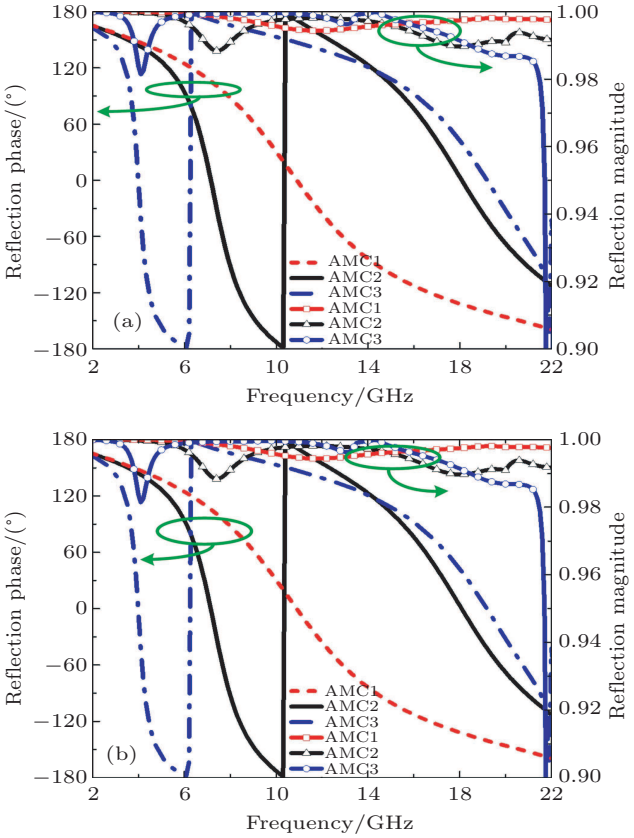


Fig. 3. (color online) Reflection characteristics of AMC1, AMC2, and AMC3 under (a) *x*-polarized incidence and (b) *y*-polarized incidence.

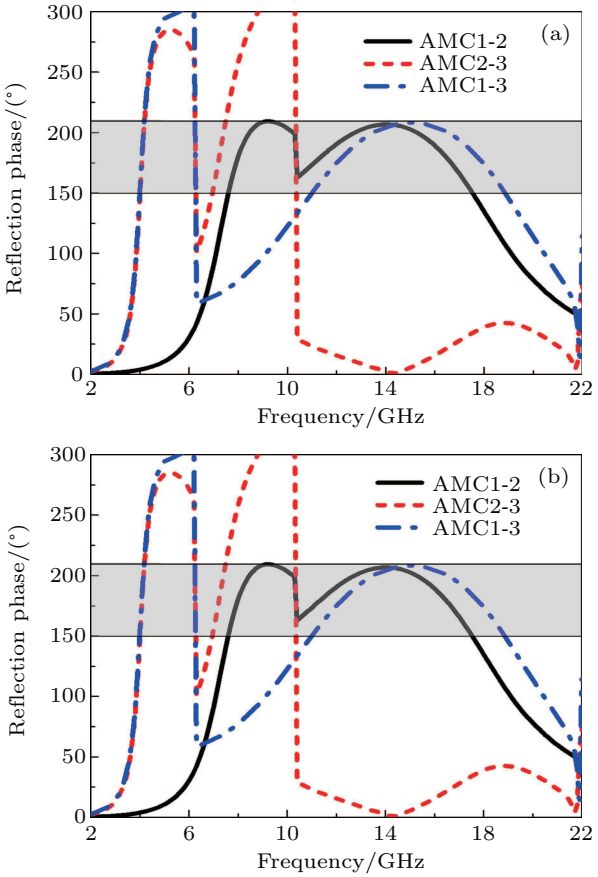


Fig. 4. (color online) Reflection phase differences between every two of the three AMC units under (a) *x*-polarized incidence and (b) *y*-polarized incidence.

Considering their application in the WGSAA, the three different AMC sub-units are arranged in a quadruple-triangle-type chessboard configuration to adapt itself to the limited room between array elements. To balance the RCSR performance in the low and high frequency bands and maximize the RCSR performance, on the basis of the simulated reflection phase difference in Fig. 4, the AMC1 is chosen as a mediator, which accounts for two-quarters of the quadruple-triangle configuration. In this way, the AMC1 tiles can be always surrounded by AMC2 and AMC3 tiles to yield required phase difference in frequency band as wide as possible as depicted in Fig. 2(b). Moreover, the proposed arrangement can significantly diminish EM echo in the specular direction and redistribute backscattered energy more uniformly in the rear hemisphere space to the benefit of the bi-static detection case. It is worth pointing out that the three AMC tiles can be arranged in other alternative configurations.

To verify the ultra-wideband low RCS capability of the proposed design, the three AMC tiles are arranged in a quadruple-triangle-type configuration to form a finite composite planar MS array with a size of 432 mm × 432 mm × 3 mm. Each AMC tile consists of sixteen optimized sub-units in a triangle-type arrangement. The simulated mono-static RCSR under normal incidence is normalized by a same-sized PEC surface as illustrated in Fig. 5. An ultra-wideband RCSR over −6 dB is observed from 4.52 GHz to 4.86 GHz (7.2% bandwidth) and from 5.9 GHz to 19.9 GHz (108.5% bandwidth). Moreover, a −3 dB RCSR is obtained nearly from 4.4 GHz to 22 GHz with a relative bandwidth of 133.3% for both x- and y-polarized incidences. The consistency between mono-static RCSR performances under the x-incidence and under the y-polarized incidence is attributed to the symmetric layout. The three-dimensional (3D) scattering patterns under normal incidence at 4.7 GHz, 10.4 GHz, and 16.8 GHz are also demonstrated in the inset. It is clearly shown that the scattered energy is redistributed into several lobes, forming a low scattering space at normal direction as a consequence. The simulated results of the finite MS array verify the capability and potentiality of our design method for ultra-wideband RCSR and bi-static RCSR to some extent.

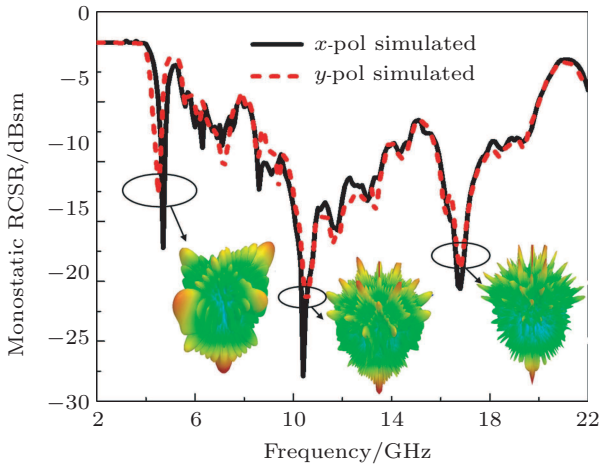


Fig. 5. (color online) Monostatic RCSR versus frequency of the composite planar MS array normalized by the same-sized PEC surface. Inset: 3D scattering patterns under normal incidence at 4.7 GHz, 10.4 GHz, and 16.8 GHz.

3. Application of MS in WGSAA radiation and scattering performance

3.1. Radiation performances

After elaborately designed and judiciously arranging the three AMC tiles, we exploit its application in WGSAA performances. In contrast to common objects, effective radiation must be assured to be a necessary condition in terms of RCSR for antenna. Therefore, we seek to maintain or even improve the radiation performance first and foremost after employing the MS. Considering the limited space to accommodate the MS, each AMC tile contains four sub-units when applied to the WGSAA. The fabricated prototype is shown in Fig. 6 with seven identical MS bars fabricated and mounted on the bare WGSAA. Each bar consists of 4 × 68 sub-units with a size of 36 mm × 615 mm. The vector network analyzer (VNA) Agilent N5230C is utilized to measure the reflection coefficient. With respect to bare WGSAA, the measured S_{11} of the MS-based antenna array is 3.165–3.297 GHz, 24 MHz broader than that of bare WGSAA, as depicted in Fig. 7. The radiation patterns of the two antennas at 3.2 GHz (the best impedance matching at this frequency for both configurations) in Fig. 8

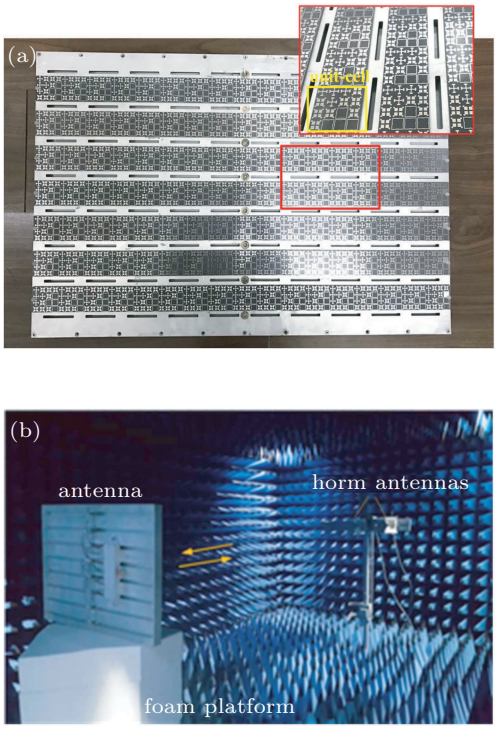


Fig. 6. (color online) Photograph of (a) fabricated WGSAA loaded with MS and (b) measurement setup.

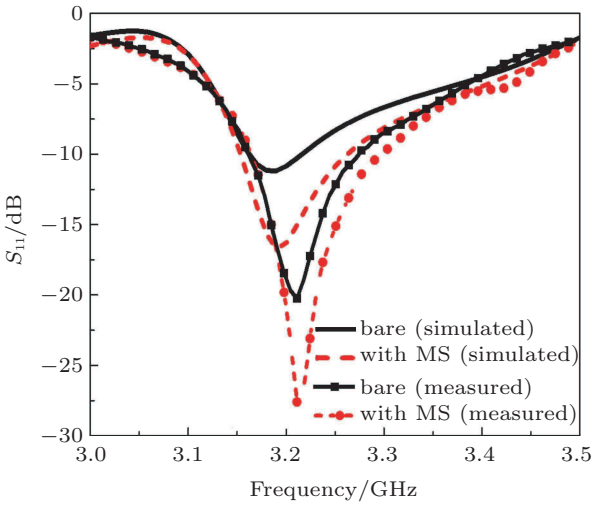


Fig. 7. (color online) Comparisons between measured and simulated S_{11} parameters.

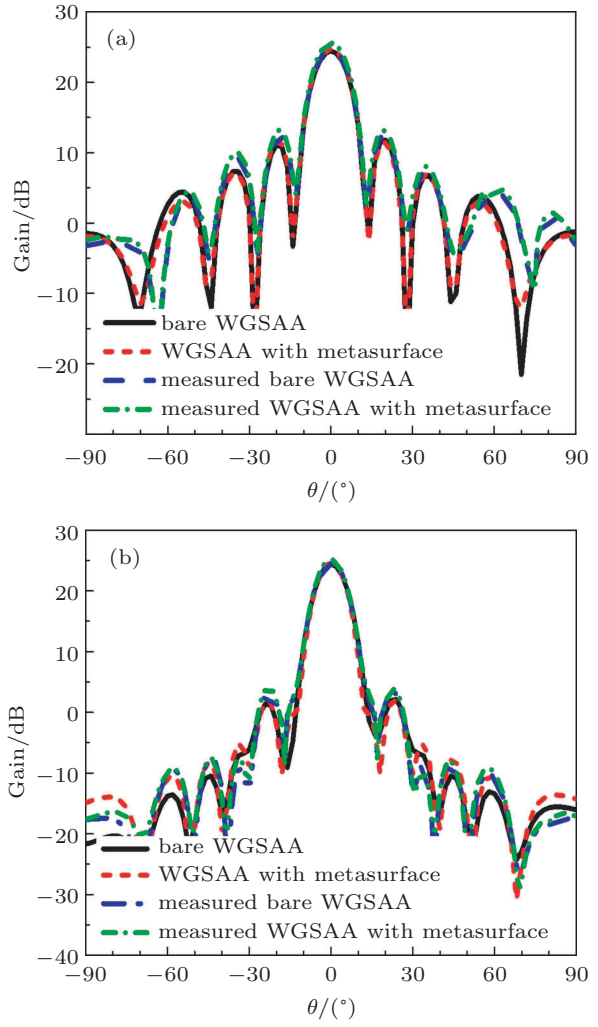


Fig. 8. (color online) Comparisons between measured and simulated radiation patterns in (a) *E*-plane (*yoz*-plane) and (b) *H*-plane (*xoz*-plane).

show that the loading of MS makes antenna gain increased by 0.77 dBi and 0.29 dBi in *E*-plane and *H*-plane, respectively. The measured results agree well with the simulation's results, which further verifies the loading of MS has little influence on antenna radiation performances.

3.2. Scattering performances

To experimentally evaluate the application of MS in scattering performance, the fabricated antenna array is measured in a microwave anechoic chamber as shown in Fig. 6(b). Two identical linear-polarized pyramidal horn antennas working at 1–18 GHz are placed adjacently as transmitter and receiver, respectively. The centers of the prototype and the two horns are at the same height and the distance between them is far enough to satisfy the far-field condition. The gate-reflect-line calibration in time-domain analysis kit of VNA is employed to further eliminate undesirable signals. The VNA Agilent N5230C is utilized to evaluate mono-static RCS value of transmission coefficients. Owing to the restriction of experimental equipment, the measured mono-static RCSR is only demonstrated in a range from 3 GHz to 18 GHz.

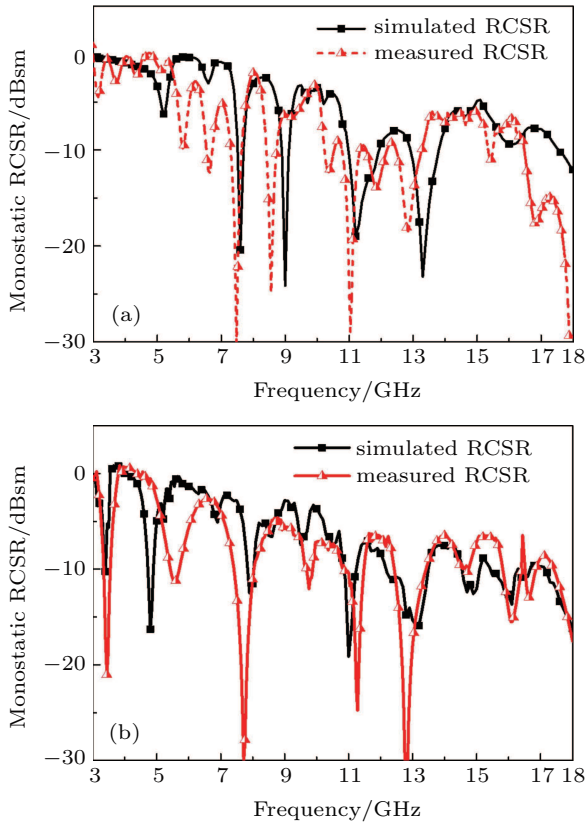


Fig. 9. (color online) Measured and simulated RCSR in comparison with bare WGSAA for (a) cross-polarization and (b) co-polarization.

As shown in Fig. 9, a continuous 6-dB RCSR is achieved from 10.12 GHz to 18 GHz and from 7.2 GHz to 18 GHz for cross- (*E*-field along *y*-axis) and co-polarized (*E*-field along *x*-axis) incidences, respectively. Meanwhile, in-band RCSR is achieved for co-polarized incidence with maximum RCSR reaching up to −5.8 dB. This is believed to be due to the co-polarized incidence inducing the slot voltage, and then leading to RCSR based on phase cancellation. Taking fabrication and measurement errors into consideration, reasonable agreement between the measured and simulated results can be found,

which confirms the effectiveness of applying MS to WGSAA for ultra-wideband RCSR.

4. Conclusions

Three kinds of PIDAMCs have been exploited and arranged in a novel quadruple-triangle-type configuration to create a composite MS, which is characterized with ultra-wideband low RCS. As a feasible application, the MS is applied to WGSAA to address the conflict between radiation and ultra-wideband low scattering performance. Both simulated and measured results verify that the proposed MS makes the antenna capable of ultra-wideband RCSR for both co- and cross-polarized incident waves without causing radiation deterioration. The proposed method can easily be applied to other antennas, especially for closely-spaced antenna arrays. Moreover, it is worth pointing out that the MS can be composed of other alternative PIDAMCs, which provides a feasible approach to invisibility of the full frequency range.

References

[1] Gomory F, Solovyov M, Souc J, Navau C, Prat-Camps J and Sanchez A 2012 *Science* **335** 1466

[2] Davenport C J and Rigelsford J M 2014 *IEEE Trans. Antennas Propag.* **62** 4518

[3] Paquay M, Iriarte J C, Ederra I, Gonzalo R and Maagt P D 2007 *IEEE Trans. Antennas Propag.* **55** 3630

[4] Zhang J, Wang J, Chen M and Zhang Z 2012 *IEEE Antennas Wireless. Propag. Lett.* **11** 1048

[5] Liu Y, Hao Y W, Li K and Gong S X 2016 *IEEE Antennas Wireless. Propag. Lett.* **15** 1028

[6] Liu Y, Li K, Jia Y T, Hao Y W, Gong S X and Guo Y J 2016 *IEEE Trans. Antennas Propag.* **64** 326

[7] Liu X, Gao J, Xu L M, Cao X Y, Zhao Y, and Li S J 2017 *IEEE Antennas Wireless Propag. Lett.* **16** 724

[8] Zhao Y, Cao X Y, Gao J and Li W Q 2014 *Microw. Opt. Technol. Lett.* **56** 158

[9] Huang C, Pan W B and Luo X G 2016 *Sci. Rep.* **6** 23291

[10] Mighani M and Dadashzadeh G 2016 *Electron. Lett.* **52** 1253

[11] Zhao Y, Cao X Y, Gao J, Yao X and Liu X 2016 *IEEE Antennas Wireless Propag. Lett.* **15** 290

[12] Simms S and Fusco V 2008 *Electron. Lett.* **44** 316

[13] Monorchio A, Manara G and Lanuzza L 2002 *IEEE Antennas Wireless Propag. Lett.* **1** 196

[14] De Cos M E, Las-Heras F and Franco M 2009 *IEEE Antennas Wireless Propag. Lett.* **8** 951

[15] ChenWG, Balanis C A and Birtcherm C R 2016 *IEEE Trans. Antennas Propag.* **64** 4133

[16] Saadat S, Adnan M, Mosallaei H and Afshari E 2013 *IEEE Trans. Antennas Propag.* **61** 1210

[17] Zheng Y J, Gao J, Cao X Y, Yuan Z D and Yang H H 2015 *IEEE Antennas Wireless Propag. Lett.* **14** 1582

[18] Chen W G, Balanis C A and Birtcher C R 2015 *IEEE Trans. Antennas Propag.* **63** 2636

[19] Iriarte J C, Pereda A T, Martinez de Falcon J L, Ederra I, Gonzalo R and Peter de Maagt 2013 *IEEE Trans. Antennas Propag.* **61** 6136

[20] Edalati A and Sarabandi K 2014 *IEEE Trans. Antennas Propag.* **62** 747

[21] Green J, Shnitkin H and Bertalan P J 1990 *IEEE Trans. Antennas Propag.* **38** 1161

[22] Cui T J, Qi M Q and Wan X 2014 *Light: Science & Applications* **3** e218